Geophysical Research Letters

RESEARCH LETTER
10.1029/2024GL114146

Unraveling the Complex Features of the Seismic Scatterers in the Mid-Lower Mantle Through Phase Transition of (Al, H)-Bearing Stishovite

Yingxin Yu[1], Youyue Zhang[2,3], Luo Li[1], Xinyue Zhang[1], Denglei Wang[1], Zhu Mao[1,4,5], Ningyu Sun[1], Yanyao Zhang[6], Xinyang Li[7], Wancai Li[8], Sergio Speziale[9], Dongzhou Zhang[10], Jung-Fu Lin[11], and Takashi Yoshino[2]

[1]Deep Space Exploration Laboratory, School of Earth and Space Sciences, University of Science and Technology of China, Hefei, China, [2]Institute for Planetary Materials, Okayama University, Misasa, Japan, [3]Geodynamics Research Center, Ehime University, Matsuyama, Japan, [4]CAS Center for Excellence in Comparative Planetology, University of Science and Technology of China, Hefei, China, [5]Frontiers Science Center for Planetary Exploration and Emerging Technologies, University of Science and Technology of China, Hefei, China, [6]Earth and Planetary Sciences, Stanford University, Stanford, CA, USA, [7]State Key Laboratory of High Pressure and Superhard Materials, College of Physics, Jilin University, Changchun, China, [8]CAS Key Laboratory of Crust-Mantle Materials and Environments, School of Earth and Space Sciences, University of Science and Technology of China, Hefei, China, [9]GFZ German Research Centre for Geosciences, Potsdam, Germany, [10]GeoSoilEnviroCARS, University of Chicago, Argonne, IL, USA, [11]Department of Earth and Planetary Sciences, Jackson School of Geosciences, The University of Texas at Austin, Austin, TX, USA

Abstract Small-scale scatterers observed in the mid-lower mantle beneath the subduction zones are thought to result from the phase transition of stishovite within subducted oceanic crusts. Here we investigate the phase transition of (Al, H)-bearing stishovite with four compositions at simultaneously high P-T conditions combining Raman spectroscopy and X-ray diffraction. These experimental results reveal that the incorporation of 0.01 a.p.f.u Al into stishovite with H/Al ratio of ~1/3 lowers the transition pressure by 6.7(3) GPa. However, the Clapeyron slope of this transition is nearly unaffected by changes in the Al content and has a value of 12.2–12.5(3) MPa/K. According to our results, Al content variation ranging from 0 to 0.07 a.p.f.u in SiO_2 can reasonably explain the depth distribution from 800 to 1,900 km of the seismic scatterers observed in the circum-Pacific region. These results deepen our understanding on the complex features of mid-lower mantle seismic scatterers and corresponding dynamic processes.

Plain Language Summary Seismic studies have identified various small-scale scatterers in the mid-lower mantle, with low-V_S and complex depth variations between 700 and 1,900 km. Understanding the formation mechanisms of these scatterers is crucial for understanding mantle dynamics and chemical evolution. Previous studies suggest that their formation is linked to the structural phase transition of SiO_2 from stishovite to post-stishovite in subducted oceanic crusts, with variations in Al and H content potentially influencing the transition depth. However, earlier experiments on (Al, H)-bearing stishovite phase transition were conducted only at high pressures and 300 K, limiting our ability to quantify the relationship between variations in subducted oceanic crust composition and small-scale scatterers in the lower mantle. In this study, we investigate the phase transition of (Al, H)-bearing stishovite under simultaneously high pressure and temperature conditions. Our results constrain how variations in Al and H content and temperature affect the transition depth. The obtained experimental results can be used to determine the depth of the post-stishovite phase transition with varying Al content at different temperatures and provide critical experimental evidence for understanding the formation and corresponding dynamic processes of small-scale scatterers in the lower mantle.

Key Points:

- The phase transition of (Al, H)-bearing stishovite are comprehensively investigated under simultaneously high P-T conditions
- Al and H incorporation into stishovite significantly lowers the transition pressure at 300 K but minimally affects the Clapeyron slope
- Al content variation from 0 to 0.07 a.p.f.u in SiO2 can explain the depth distribution of seismic scatterers in the circum-Pacific region

Supporting Information:

Supporting Information may be found in the online version of this article.

Correspondence to:

Y. Zhang and Z. Mao,
zhang.youyue.rn@ehime-u.ac.jp;
zhumao@ustc.edu.cn

Citation:

Yu, Y., Zhang, Y., Li, L., Zhang, X., Wang, D., Mao, Z., et al. (2025). Unraveling the complex features of the seismic scatterers in the mid-lower mantle through phase transition of (Al, H)-bearing stishovite. *Geophysical Research Letters*, *52*, e2024GL114146. https://doi.org/10.1029/2024GL114146

Received 8 DEC 2024
Accepted 1 JUL 2025

Author Contributions:

Conceptualization: Yingxin Yu, Youyue Zhang, Luo Li, Xinyue Zhang, Ningyu Sun, Yanyao Zhang, Xinyang Li, Wancai Li, Sergio Speziale, Jung-Fu Lin, Takashi Yoshino
Data curation: Yingxin Yu, Youyue Zhang, Luo Li, Xinyue Zhang, Denglei Wang, Ningyu Sun, Yanyao Zhang, Xinyang Li, Wancai Li, Sergio Speziale, Dongzhou Zhang, Jung-Fu Lin, Takashi Yoshino
Formal analysis: Yingxin Yu, Youyue Zhang, Luo Li, Xinyue Zhang, Ningyu Sun, Xinyang Li, Sergio Speziale

1. Introduction

Short-period seismic waves have revealed the ubiquitous presence of small-scale seismic scatterers in the mid-lower mantle (Kaneshima & Helffrich, 1999; Krüger et al., 2001; Niu, 2014; Rost et al., 2008). Most of them are detected beneath the subduction zone, with occasional observations near hotspots (Haugland et al., 2017; Kaneshima, 2019, 2023; Yuan et al., 2021). These seismic scatterers are characterized by a shear velocity reduction of 2%–12% and a planar geometry, with thickness ranging from several to tens of kilometers and lateral extents spanning tens to hundreds of kilometers. (Haugland et al., 2017; Kaneshima, 2019; Niu, 2014; Niu

Funding acquisition: Youyue Zhang, Jung-Fu Lin, Takashi Yoshino
Investigation: Yingxin Yu, Youyue Zhang, Luo Li, Xinyue Zhang, Denglei Wang, Ningyu Sun, Yanyao Zhang, Xinyang Li, Sergio Speziale, Dongzhou Zhang, Jung-Fu Lin, Takashi Yoshino
Methodology: Yingxin Yu, Youyue Zhang, Luo Li, Xinyue Zhang, Ningyu Sun, Yanyao Zhang, Xinyang Li, Wancai Li, Sergio Speziale, Dongzhou Zhang, Takashi Yoshino
Project administration: Youyue Zhang
Resources: Xinyang Li, Wancai Li, Sergio Speziale, Jung-Fu Lin, Takashi Yoshino
Software: Yingxin Yu, Xinyue Zhang
Supervision: Sergio Speziale
Validation: Yingxin Yu, Youyue Zhang, Ningyu Sun, Yanyao Zhang, Takashi Yoshino
Visualization: Yingxin Yu, Denglei Wang
Writing – original draft: Yingxin Yu, Youyue Zhang, Luo Li, Xinyue Zhang, Ningyu Sun, Yanyao Zhang, Xinyang Li, Sergio Speziale
Writing – review & editing: Yingxin Yu, Youyue Zhang, Luo Li, Xinyue Zhang, Denglei Wang, Ningyu Sun, Yanyao Zhang, Xinyang Li, Wancai Li, Sergio Speziale, Dongzhou Zhang, Jung-Fu Lin, Takashi Yoshino

et al., 2003). Furthermore, these seismic scatterers exhibit a complex depth distribution, with over 70% located at depths of 700–1,300 km, approximately 20% between 1,300 and 1,900 km, and less than 10% observed at depths greater than 1,900 km (Kaneshima, 2016; Li et al., 2022). The complicated features of these scatterers make it challenging to fully understand their origin and corresponding dynamic processes.

The subducted oceanic crusts are regarded as the major source of lower-mantle heterogeneity (Kaneshima & Helffrich, 1999; Wang et al., 2020). Free silica (SiO_2) is a notable phase in the subducted oceanic crusts, constituting 16%–25% of the volume (Hirose et al., 2005; Ishii, Miyajima, et al., 2022; Ricolleau et al., 2010). In the shallow lower mantle, it is stable in the form of stishovite (stv) with a rutile-type structure and then transitions into $CaCl_2$-type post-stishovite (post-stv) at ∼55 GPa and 300 K with a positive Clapeyron slope of 11.1–15.4 MPa/K (Fischer et al., 2018; Hirose et al., 2005; Kingma et al., 1995; Nomura et al., 2010; Ono et al., 2002; Shieh et al., 2005; Yamazaki et al., 2014). This transition causes notable shear velocity softening and has been regarded as the potential cause for the observed mid-lower mantle scatterers (Andrault et al., 1998; Carpenter et al., 2000; Hemley et al., 2000; Zhang et al., 2021). However, even when accounting for the temperature variations within the lower mantle, the post-stishovite transition of pure SiO_2 cannot satisfy the wide depth distribution of the observed seismic scatterers from 700 to 1,900 km.

It should be noted that the subducted oceanic crust contains up to ∼19 wt.% Al_2O_3, which can partition into stishovite via the substitution mechanism of $2Al^{3+} + O_V^{2+} = 2Si^{4+}$ (Ono et al., 2001; Pawley et al., 1993). Also, H^+ can be incorporated into stishovite by the coupled substitution with Al^{3+} or direct substitution of $4H^+ \rightarrow Si^{4+}$ (Bromiley et al., 2006; Litasov et al., 2007; Pawley et al., 1993). Previous studies have demonstrated that the incorporation of a certain amount of Al and H into stishovite can effectively lower the transition pressure to the post-stishovite phase, making it more consistent with the depths of seismic scatterers in the lower mantle (Criniti et al., 2023; Lakshtanov, Sinogeikin, et al., 2007; Zhang et al., 2022). For example, stishovite with ∼4 wt.% Al_2O_3 transitions into the post-stishovite phase at 23–24 GPa and 300 K (Bolfan-Casanova et al., 2009). The transition pressure for stishovite with 5.37 wt.% Al_2O_3 and 0.27 wt.% H_2O at 300 K is as low as 16.1 GPa (Zhang et al., 2022). While Lakshtanov, Sinogeikin, et al. (2007) propose a linear decrease in phase transition pressure with increasing Al content, more recent research suggests a polynomial relationship between Al content and transition pressure (Zhang et al., 2022). Notably, these previous studies only decipher the relationship between transition pressure reduction and Al content in stishovite at 300 K, and the combined effects of composition and temperature on the phase boundary of the post-stishovite transition still remain poorly understood, significantly limiting our understanding on the complex features of mid-lower mantle scatterers (Bolfan-Casanova et al., 2009; Criniti et al., 2023; Lakshtanov, Sinogeikin, et al., 2007; Zhang et al., 2022).

In this study, we comprehensively investigated the net effect of Al and H on the phase transition and equation of state (EoS) of stishovite by combining Raman spectroscopy and single-crystal X-ray diffraction (XRD). Raman spectroscopy was applied to determine the phase boundary between (Al, H)-bearing stishovite and post-stishovite at simultaneously high pressures and temperatures, while single-crystal XRD provided crucial constraints on the variation of lattice parameters across the phase transition at high pressures and 300 K. These experimental results allow us to constrain the impact of the compositional variation on the phase boundary of stishovite at simultaneously high P-T conditions. These results deepen our understanding of the complex characteristics of the lower-mantle seismic scatterers.

2. Experiments

Single-crystal stishovite with four different compositions was synthesized by a large-volume press (LVP) at the Institute for Planetary Materials, Okayama University. The composition of the starting materials and recovered sample, as well as the synthesis conditions, have been summarized in Table S1 in Supporting Information S1 and described Text S1 in Supporting Information S1. The composition of the synthesized samples was determined by electron probe microanalyzer (EPMA) in the Key Laboratory of Crust-Mantle Materials and Environments, University of Science and Technology of China (USTC) (Tables S1 and S2 in Supporting Information S1). The unpolarized infrared spectra collected by the micro-Fourier Transform Infrared (FTIR) spectrometer in the Key Laboratory of Crust-Mantle Materials and Environments in USTC were used to determine the H_2O content of these recovered samples (Figure S1 in Supporting Information S1). To better compare with previous studies, we also use the calibration method by Paterson (1982) to evaluate the H_2O content (Table S1, Figure S1, and Text S1 in Supporting Information S1). The samples used in this study are hereafter named Al2.5-SiO_2, Al5.1-SiO_2,

Al5.9-SiO_2, and Al0-SiO_2 according to the chemical compositions (Table S1 and Figure S2 in Supporting Information S1).

High P-T Raman measurements up to 66 GPa and 700 K were performed using the membrane-driven externally heated diamond anvil cells (DACs) at the High Pressure and Temperature Mineral Physics Laboratory at USTC and State Key Laboratory of Superhard Materials at Jilin University. The Raman system is equipped with a 532 nm-wavelength green laser. For measurements under high pressure and 300 K, four single-crystal samples in different compositions, which have been double-side polished to 10–15 μm in thickness and cut to ~20 μm in diameter, were loaded into each sample chamber in DACs equipped with a pair of diamonds with culets of 300 or 200 μm. 250-μm thick Re foil was pre-indented to ~35 μm in thickness, and a hole with a diameter of 160 or 110 μm was drilled to serve as the sample chamber. Ne was used as the pressure-transmitting medium. Ruby was placed next to the sample platelets and used as the pressure calibrant for the experiments under high pressure and 300 K (Datchi et al., 2007). At 300 K, Raman spectra were collected up to 66 GPa (Figure S3 in Supporting Information S1). High P-T experiments were conducted using BX90 DACs (Kantor et al., 2012). High temperature was generated by platinum-rhodium alloy resistive heaters. A K-type thermocouple attached to the diamond surface ~500 μm away from the diamond culet was used to determine the temperature. The uncertainty of the temperature measurements in our BX90 DACs was within ±5 K (Sinogeikin et al., 2006). Ruby and Sm^{2+}: SrB_4O_7, placed next to the samples, served as the pressure calibrant during high P-T experiments, and the difference in pressure determined by Ruby and Sm^{2+}: SrB_4O_7 is less than 1 GPa at the investigated pressure range (Datchi et al., 2007). Due to the overlap of R_1 and R_2 lines of ruby above 600 K, the pressure is only determined by Sm^{2+}: SrB_4O_7 for the experiments at 700 K. High-temperature isothermal compressions were carried out at 400, 500, 600, and 700 K, respectively, and the pressure step was 1–2 GPa up to ~50 GPa. Each Raman spectrum was collected by a 20X objective with a focused beam diameter of 3 μm, a typical exposure time of 15 s, and 5 accumulations (Figures S3 and S4 in Supporting Information S1). The laser power used to generate the Raman signal is 200 mW.

Single-crystal XRD experiments under high pressure and 300 K were performed at the beamline 13-BM-C of the GSECARS, Advanced Photon Source (APS), Argonne National Laboratory, and the Extreme Conditions Beamline (P02.2) at PETRA III, DESY. The wavelength of the X-ray was 0.4340 Å for 13-BM-C at APS and 0.2910 Å for P02.2 at PETRA III. Short symmetric DACs with 300-μm culets were used for high-pressure XRD measurements. The gasket and pressure transmitting medium are the same as those of the high P-T Raman measurement experiments. For each (Al, H)-bearing sample, two sample platelets with different crystallographic orientations were loaded into the same sample chamber. One piece of Au foil placed next to the sample platelets served as the pressure calibrant (Fei et al., 2007). A ruby sphere was also loaded into the sample chamber to determine the pressure during gas loading. We collected the XRD data at an interval of 1–2 GPa up to 57 GPa (Figure S5 in Supporting Information S1). At each pressure, the sample stage was rotated ±35° along its vertical axis to detect as many diffraction spots as possible.

3. Results

3.1. High P-T Raman Results

At ambient conditions, four major optic modes at ~230, ~585, ~750, and ~950 cm^{-1} were observed for all our stishovite samples in the four different compositions, which can be assigned to B_{1g}, E_g, A_{1g}, and B_{2g} modes, respectively (Figure 1a, Figures S3 and Tables S3–S6 in Supporting Information S1) (Kingma et al., 1995). The frequencies of each optic mode slightly decrease with the increased Al content. The intensity of the B_{2g} mode weakens with pressure, and it is difficult to detected for all the samples. For comparison, we only analyzed the variation of Raman shift for modes B_{1g}, E_g, and A_{1g} with pressure for all the four compositions (Figure 1 and Tables S3–S6 in Supporting Information S1). In general, the frequencies of E_g and A_{1g} modes exhibit a nearly linear increase with pressure for all the investigated compositions, while the B_{1g} mode exhibits obvious softening with increasing pressure. Above 18 GPa, the pressure dependence of the frequency of the B_{1g} mode of stishovite becomes positive for Al5.9-SiO_2, which indicates the phase transition from stishovite to post-stishovite. Accompanied by this, the slope of E_g and A_{1g} modes slightly changes. After the post-stishovite transition, B_{1g} and A_{1g} modes both convert into the A_g mode, and the E_g mode transforms into a B_{2g} mode of the post-stishovite phase. We observed a similar change at ~21.8 GPa for Al5.1-SiO_2, ~37.5 GPa for Al2.5-SiO_2, and 55.2 GPa for Al0-SiO_2. With the temperature increasing, the turning of B_{1g} mode occurs at a higher pressure for all three

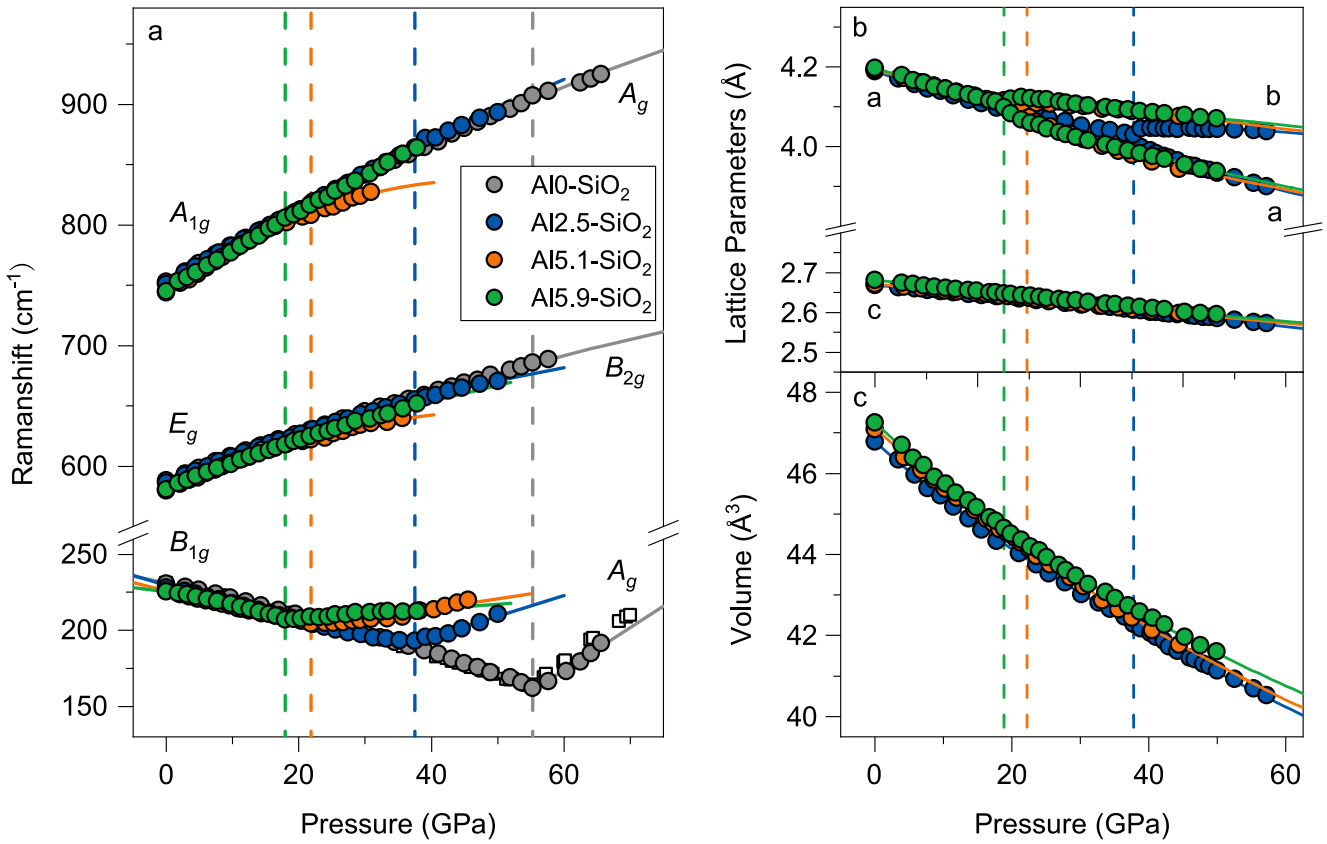

Figure 1. The experimental results in this study. (a) Raman shifts of (Al, H)-bearing stishovite at high pressure and 300 K. Gray: Al0-SiO_2; blue: Al2.5-SiO_2; orange: Al5.1-SiO_2; green: Al5.9-SiO_2. Solid lines: the best linear or quadratic fitting results of our experimental data. Open squares: Zhang et al. (2021). (b) and (c) Lattice parameters and equation of state (EoS) of (Al, H)-bearing stishovite at high pressure and 300 K. Solid lines: fitting results by the third-order Birch-Murnaghan EoS. Vertical dashed lines: transition pressure of each sample.

(Al, H)-bearing samples (Figure S4 in Supporting Information S1). For Al5.9-SiO_2, the pressure at which the pressure dependence of B_{1g} mode becomes positive is ~19.4 GPa at 400 K, and shifts to ~22.6 GPa at 700 K. Similar changes are also observed for the other two (Al, H)-bearing samples, with the kink in the B_1g mode increasing in pressure by 1.1–1.4 GPa for every 100 K rise in temperature.

3.2. Lattice Parameter and Equation of State (EoS)

The collected XRD patterns of all (Al, H)-bearing samples at 300 K show 9–15 reflections (Figure S6 in Supporting Information S1). With the increasing pressure, the observed 210, 211, 310, 311, 420, and 421 reflections for Al5.9-SiO_2 and 101, 210, and 211 reflections for Al5.1-SiO_2 in the tetragonal structure split into a doublet above ~18.9 and ~22.5 GPa, respectively. Similar splitting of 211, 202, 212, and 321 reflections for Al2.5-SiO_2 was observed at ~38.8 GPa. The splitting of these observed peaks indicates the transition from stishovite with tetragonal structure to post-stishovite with orthorhombic structure. We thus analyzed the higher-pressure XRD patterns using the orthorhombic structure of the post-stishovite phase (Tables S7–S9 in Supporting Information S1). We showed that the *a*-axis of Al2.5-SiO_2, Al5.1-SiO_2, and Al5.9-SiO_2 split into *a*- and *b*-axis at 38.8, 22.5, and 18.9 GPa, respectively. Across this phase transition, the pressure dependence of *c* and *V* slightly changes (Figure 1 and Tables S7–S9 in Supporting Information S1). Given the well-known trade-off between isothermal bulk modulus (K_{T0}) and its pressure derivative (K_{T0}') in XRD measurements, we derive the isothermal bulk modulus (K_{T0}) with the fixed K_{T0}' of 4 using Birch-Murnaghan EoS for each sample. The obtained K_{T0} decreases with increasing Al content (Table S10 in Supporting Information S1).

4. Discussion

4.1. Post-Stishovite Transition at High P-T

Previous studies have shown that SiO_2 undergoes a second-order ferroelastic transition from stishovite to the $CaCl_2$-type post-stishovite at 50–55 GPa and 300 K (Andrault et al., 2003; Carpenter et al., 2000; Kingma et al., 1995; Zhang et al., 2021). This transition is manifested by a softening of the B_{1g} mode of stishovite from Raman measurements (Kingma et al., 1995; Zhang et al., 2021). After the transition into post-stishovite, the B_{1g} mode transforms into the A_g mode, and its frequency starts to increase with pressure. Meanwhile, the E_g mode across the phase transition will split into the B_{2g} and B_{3g} modes (Kingma et al., 1995). However, the splitting of the E_g mode was not identified in our Raman measurements due to its relatively low intensity (Figure 1 and Figures S3 and S4 in Supporting Information S1). Therefore, the transition pressure from stishovite to post-stishovite in this study was determined by the intersection of squared Raman shifts of the B_{1g} and A_g mode (Figure S5 in Supporting Information S1).

At 300 K, the intersection of squared Raman shifts of B_{1g} and A_g mode for Al0-SiO_2 occurs at 55.4(4) GPa, which is consistent with previous studies (Andrault et al., 1998; Kingma et al., 1995; Zhang et al., 2021). For three (Al, H)-bearing stishovite samples, the transition pressure was determined as 38.0(6) GPa for Al2.5-SiO_2, 21.8(4) GPa for Al5.1-SiO_2, and 18.0(4) GPa for Al5.9-SiO_2, respectively, visibly lower than that of endmember stishovite. In addition, across the post-stishovite transition, the Wyckoff position of oxygen atoms would split, thus causing a symmetry reduction from tetragonal to orthorhombic (Zhang et al., 2023). Therefore, the transition pressure could also be determined by the intersection of the linear extrapolation of a straight line of the squared symmetry-breaking strains from the lattice parameters $(e_1\text{-}e_2)^2$ and the pressure axis according to the Landau theory (Figure S7 in Supporting Information S1) (Carpenter et al., 2000). This yields a transition pressure of 37.1(8) GPa for Al2.5-SiO_2, 21.4(6) for Al5.1-SiO_2, and 17.3(6) for Al5.9-SiO_2, respectively, consistent with that determined by softening of the B_{1g} mode.

For (Al, H)-bearing stishovite, part of Al^{3+} incorporates into stishovite by the oxygen vacancy substitution of the $AlO_{1.5}$ component, while the other part incorporates into stishovite via charge-coupled substitution of AlOOH component (Bromiley et al., 2006; Pawley et al., 1993). We have noted that the H/Al ratio of stishovite used in this study and most of the previous studies is close to 1/3, making it difficult to isolate the individual effects of these two substitution mechanisms (Figure S2 in Supporting Information S1). Nevertheless, these results provide a robust constraint on the combined effect of Al and H incorporation on the phase boundary of stishovite while the H/Al ratio is ∼1/3. We thus derived the relationship between transition pressure at 300 K and Al content in stishovite with the H/Al ratio of ∼1/3 as follows (Figure 2):

$$P_{tr} = 55(2) - 6.7(3) \times Al \times 100 \quad (1)$$

where P_{tr} represents the transition pressure in units of GPa, Al is atom per formula unit (a.p.f.u). According to our modeling result, the incorporation of 0.01 a.p.f.u Al could reduce the transition pressure by 6.7(3) GPa, when the H/Al ratio in stishovite is ∼1/3. It is important to note that our experimental results show a linear decrease in the phase transition pressure of stishovite at 300 K with increasing Al content, rather than the polynomial trend reported by Zhang et al. (2022). These differences are mainly due to the more diverse H/Al ratio of their samples. Specifically, sample Al4.0-SiO_2 from Zhang et al. (2022) has a H/Al ratio of 0.41(8), which is apparently higher than 1/3, thus causing it to deviate from the linear relationship we obtained.

More importantly, we provide experimental constraints on the influence of temperature on the phase transition pressure of (Al, H)-bearing stishovite based on the Raman shifts of the B_{1g} mode. The phase diagram of three (Al, H)-bearing stishovite samples is shown in Figure 3. The transition pressure of each sample increases with the temperature, which indicates the positive Clapeyron slopes of this transition. We thus determined the Clapeyron slopes of each phase as 12.5(3) MPa/K for Al2.5-SiO_2, 12.4(3) MPa/K for Al5.1-SiO_2, and 12.2(3) MPa/K for Al5.9-SiO_2, respectively, which is similar to that of pure stishovite of 11.1–15.4 MPa/K (Fischer et al., 2018; Nomura et al., 2010; Ono et al., 2002). Therefore, our results reveal that the incorporation of Al and H into stishovite significantly reduces the transition pressure but has a minor effect on the Clapeyron slopes. When the H/Al ratio in stishovite is ∼1/3, the combined effect of composition and temperature on the post-stishovite transition pressure can be described as:

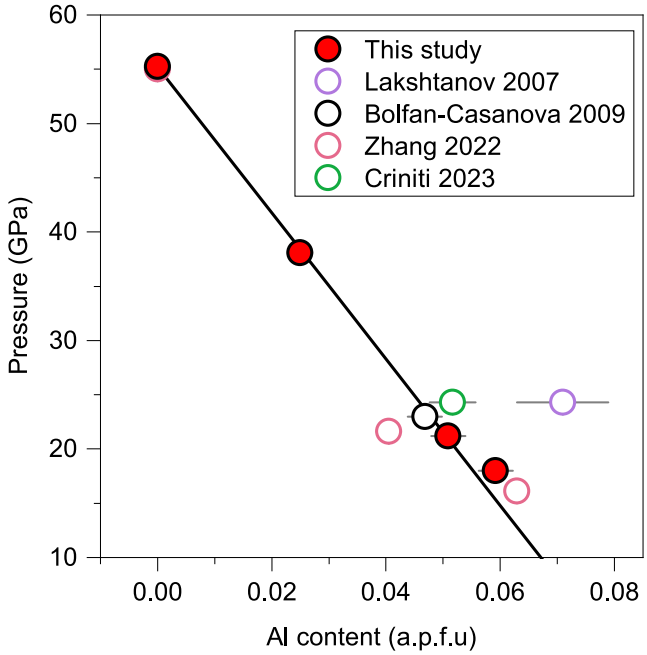

Figure 2. The effect of Al content on the post-stishovite transition pressure at 300 K. Red: this study; purple: Lakshtanov, Sinogeikin, et al. (2007); black: Bolfan-Casanova et al. (2009); pink: Zhang et al. (2022); green: Criniti et al. (2023). Solid line: the transition pressure as a function of Al content when the H/Al ratio in stishovite is ~1/3; Error bars smaller than the symbols are not shown.

$$P_{tr} = 55(2) - 6.7(3) \times Al \times 100 + 0.0123(3) \times (T - 300) \quad (2)$$

where is Al is expressed in a.p.f.u, and T is in units of K.

4.2. Origin for the Depth Variation of Mid Lower-Mantle Scatterers

The mid-lower mantle seismic scatterers are characterized by the complex depth distribution (Haugland et al., 2017; Kaneshima, 2016; Li et al., 2022; Yuan et al., 2021; Zhang et al., 2020). Especially for the circum-Pacific region, most observed seismic scatterers are shallower than 1,400 km, with deeper scatterers (>1,400 km) primarily concentrated in the Tonga-Fiji region (e.g., Kaneshima, 2019; Li & Yuen, 2014; Niu, 2014). To understand the complex depth variation of mid-lower mantle seismic scatterers, we comprehensively model the effect of composition and temperature variations on the phase transition of stishovite in the lower mantle (Figure 4). In our modeling, the H/Al ratio is close to 1/3, and we allowed Al content to vary in SiO_2. The model established based on our latest experimental constraints of the phase boundary can be used to determine the depth at which the post-stishovite phase transition occurs in SiO_2 with varying Al content at different temperatures (Figure 4 and Figure S9 in Supporting Information S1).

Along the normal mantle geotherm, the post-stishovite transition occurs at ~1,860 km (~80 GPa) for the Al-free stishovite (Figure 4a). Elevating the Al content in stishovite causes the post-stishovite transition to shift to shallower depth. For example, stishovite with 0.03 a.p.f.u (1 mol.%) Al in the subducted oceanic crusts undergoes the post-stishovite transition at ~1,410 km (~58 km). For a higher Al content of 0.06 a.p.f.u (2 mol.%) in SiO_2, the post-stishovite transition occurs even shallower, at depths of ~940 km, while up to 0.07 a.p.f.u Al reduces the transition depth to 800 km. Along the cold slab geotherm, which is 500-K colder than the normal mantle, the post-stishovite transition shifts to a shallower depth with a given Al content. For stishovite with 0.03 and 0.06 a.p.f.u Al, the post-stishovite transition occurs at 1,250 and 800-km depth, respectively. Here, we also estimated the effect of experimental uncertainty on the phase transition depth (Figure S9 in Supporting Information S1). We found that, at a given Al content, the experimental uncertainty associated with our derived parameters can lead to a variation of 40–80 km in the transition depth. Moreover, since our experiments were conducted at relatively low temperatures, extrapolating our results to mantle conditions may also introduce additional uncertainty. Therefore, we also referred to the Clapeyron slopes of pure SiO_2 determined from previous

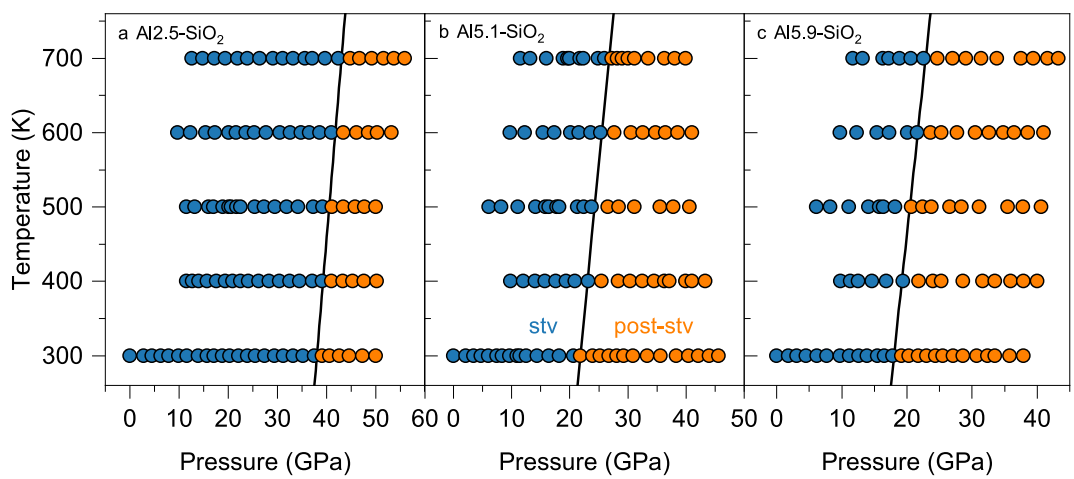

Figure 3. Phase diagram of (Al, H)-bearing stishovite at high P-T. (a) Al2.5-SiO_2; (b) Al5.1-SiO_2; (c) Al5.9-SiO_2. Blue: stishovite; orange: post-stishovite. Solid lines: phase boundary between stishovite and post-stishovite.

10.1029/2024GL114146

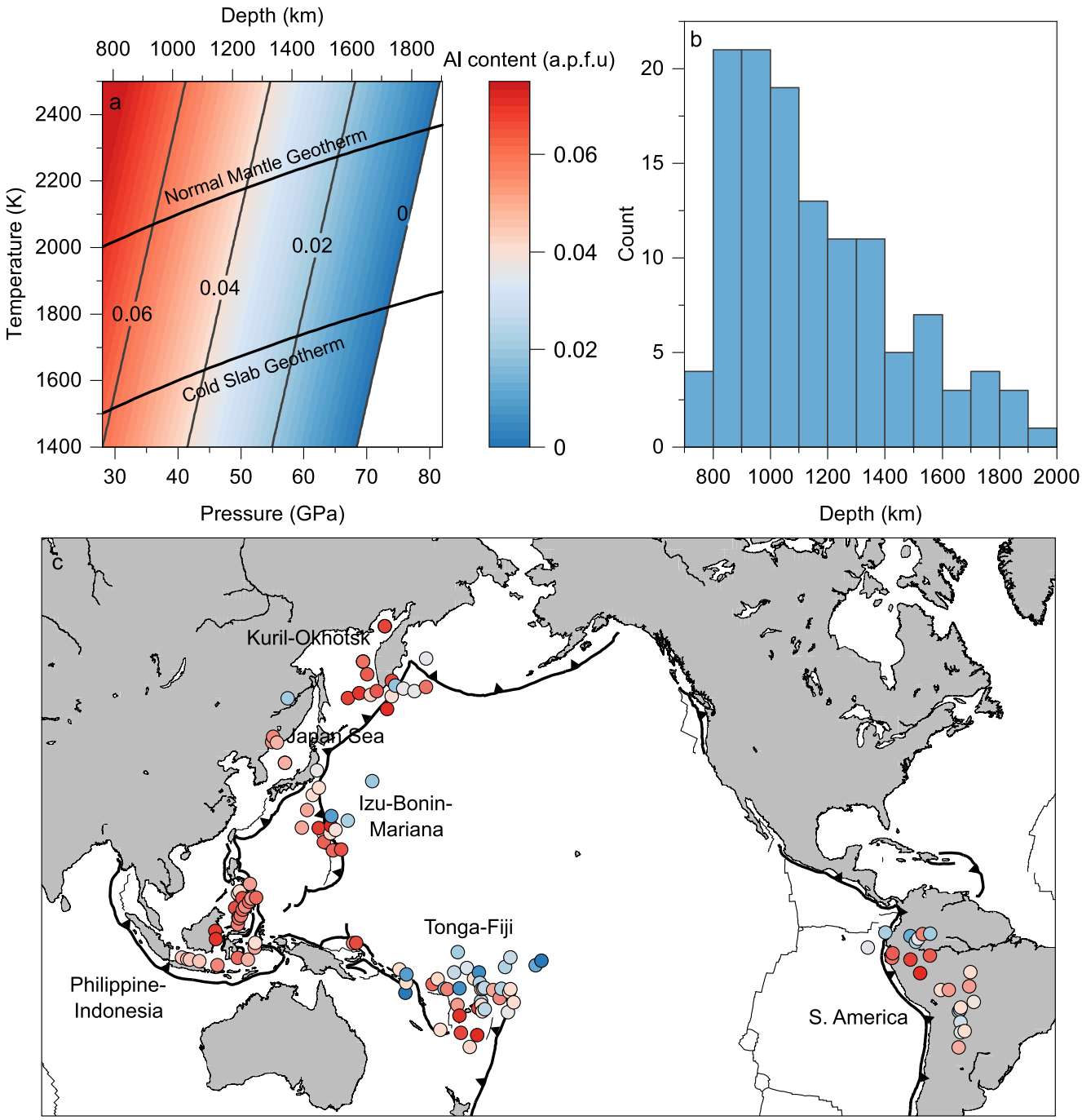

Figure 4. (a) The phase boundary between stishovite and post-stishovite with the varying Al content. The contour represents the phase boundary of stishovite with different Al content and the Al/H ratio of 1/3. Geotherm: From Katsura (2022). (b) The depth distribution histogram of the lower-mantle seismic scatterers in the circum-Pacific region (He & Zheng, 2018; Kaneshima, 2019; Li & Yuen, 2014; Niu, 2014; Niu et al., 2003; Vanacore et al., 2006; Yang & He, 2015; Yuan et al., 2021). (c) Map of the mid-lower mantle scatterers around the circum-Pacific region. The color of these spots represents the Al content in SiO_2 required to account for the observed depth of these seismic scatterers. The Al content in SiO_2 was estimated under the conditions of the H/Al ratio of 1/3 and the normal mantle geotherm. The color bars in figures a and c are the same.

laser-heating experiments (Fischer et al., 2018; Nomura et al., 2010; Ono et al., 2002). Taking the experimental results of Nomura et al. (2010) and Fischer et al. (2018) as the lower and upper bounds of the Clapeyron slope for the structural transition in SiO_2, we found that, at a given Al content of 0.06 a.p.f.u, using different Clapeyron slopes results in a variation of ~200 km in the transition depth (Figure S10 in Supporting Information S1).

Actually, the Al content in stishovite in the subducted oceanic crust is likely governed by partitioning among coexisting phases, which might be affected by temperature and the presence of H_2O. In the cold slab, δ-AlOOH and aluminous phase D may coexist with stishovite and bridgmanite and result in the depletion of Al in them, leading to a greater phase transition depth of stishovite (Ishii et al., 2024; Ishii, Ohtani, et al., 2022; Liu et al., 2019). Such a scenario reasonably explain that the seismic scatterers deeper than 1,400 km mainly concentrate in the Tonga slab, which is one of the coldest slabs (Figure 4c) (Ganguly et al., 2009). In contrast, most slabs stagnating at the bottom transition zone or top lower mantle may be continuously heated, leading to the release of Al and H from Al-bearing hydrous minerals (Chen et al., 2025; Fukao & Obayashi, 2013; Goes et al., 2017). The released Al and H could be incorporated into SiO_2 and shift the post-stishovite transition to shallower depths, accounting for the shallower seismic scatters detected at the regions with slab stagnation, such as the western Pacific region. Also, the widespread slab stagnation results in more than 70% of seismic scatterers concentrated at depths of 800–1,300 km (Figure 4b). Therefore, depending on the thermal and dynamical state of the subducted slab, stishovite in the subducted oceanic crusts may contain varying amounts of Al and H, leading to variations in the transition depth. This depth variation provides a plausible explanation for the presence of small-scale seismic scatterers observed at 800–1,900 km depths. Despite these insights, experimental constraints on the elasticity of (Al, H)-bearing stishovite under simultaneously high P-T conditions remain limited (Lakshtanov, Litasov, et al., 2007; Zhang et al., 2022). Future elasticity measurements, combined with our experimental constraints on the phase boundary of post-stishovite transition, are expected to provide a more comprehensive understanding of the complex depth and low-velocity anomalies of small-scale seismic scatterers in the mid-lower mantle.

5. Conclusion

In this study, we investigated the phase transition and elasticity of (Al, H)-bearing stishovite by Raman spectroscopy and synchrotron XRD at high pressures and temperatures. Specifically, we provide crucial constraints on how the variation in Al and H contents and temperature on the post-stishovite phase transition pressure. Our results indicate that the incorporation of 0.01 a.p.f.u Al into stishovite with H/Al ratio of ∼1/3 could lower the post-stishovite transition pressure by 6.7(3) GPa at 300 K. However, the variation in Al and H content in stishovite have a negligible effect on the Clapeyron slopes. Based on these results, we further model the effect of composition and temperature variations on the transition depth of stishovite in the lower mantle. For the Al-free SiO_2, the post-stishovite transition occurs at ∼1,860 km, while the incorporation of 0.07 a.p.f.u (2.3 mol.%) Al can shift the transition depth to ∼800 km, thus reasonably explaining the wide depth distribution of the seismic scatterers in the circum-Pacific region. Our findings provide essential information for understanding the complex depth characteristics of small-scale scatterers in the mid-lower mantle.

Conflict of Interest

The authors declare no conflicts of interest relevant to this study.

Data Availability Statement

Data generated in this study can be found in the online Supporting Information S1. They can also be downloaded online Yu et al. (2025) (from https://doi.org/10.5281/zenodo.15590899).

Acknowledgments
We acknowledge T. Xiao for EPMA measurements, Y. Wei and X. Wei for their assistance with the experiments conducted at Jilin University, and T. Ishii for constructive discussion. This work is supported by the National Natural Science Foundation of China (42425202, 42272036 and 42241117), National Key R&D Program of China (2023YFF0803200), the Fundamental Research Funds for the Central Universities (WK2080000189), and the Ministry of Education, Culture, Sports, Science, and Technology of the Japanese Government (21H04996 and 24K17148). JFL acknowledges support from the Geophysics Program of the National Science Foundation of the US (EAR-2333879). XRD data for the Al5.1-SiO_2 sample were collected at 13-BM-C of the Advanced Photon Source, Argonne National Laboratory (proposal 2022-GUP-BM-80436), which is supported by the National Science Foundation-Earth Sciences (EAR-1661511 and EAR-1634415) and Department of Energy (DE-FG02-94ER14466 and DE-AC02-06CH11357). XRD data for Al2.5-SiO_2 and Al5.9-SiO_2 were collected at beamline P02.2 of PETRA III (proposal I-20230916), and we would like to thank H.P. Liermann for assistance in using P02.2 and his constructive comments on our manuscript. We acknowledge DESY (Hamburg, Germany), a member of the Helmholtz Association HGF, for the provision of experimental facilities. This work was partially carried out at the high-pressure synergetic measurement station of Synergic Extreme Condition User Facility.

References

Andrault, D., Angel, R. J., Mosenfelder, J. L., & Le Bihan, T. (2003). Equation of state of stishovite to lower mantle pressures. *American Mineralogist*, *88*(2–3), 301–307. https://doi.org/10.2138/am-2003-2-307

Andrault, D., Fiquet, G., Guyot, F., & Hanfland, M. (1998). Pressure-induced Landau-type transition in stishovite. *Science*, *282*(5389), 720–724. https://doi.org/10.1126/science.282.5389.720

Bolfan-Casanova, N., Andrault, D., Amiguet, E., & Guignot, N. (2009). Equation of state and post-stishovite transformation of Al-bearing silica up to 100 GPa and 3000 K. *Physics of the Earth and Planetary Interiors*, *174*(1–4), 70–77. https://doi.org/10.1016/j.pepi.2008.06.024

Bromiley, G. D., Bromiley, F. A., & Bromiley, D. W. (2006). On the mechanisms for H and Al incorporation in stishovite. *Physics and Chemistry of Minerals*, *33*(8–9), 613–621. https://doi.org/10.1007/s00269-006-0107-9

Carpenter, M. A., Hemley, R. J., & Mao, H. k. (2000). High-pressure elasticity of stishovite and the $P4_2/mnm \rightleftharpoons Pnnm$ phase transition. *Journal of Geophysical Research*, *105*(B5), 10807–10816. https://doi.org/10.1029/1999jb900419

Chen, L., Liu, Z., Zhao, X., Xu, C., Ju, D., Feng, B., et al. (2025). Water solubility in nominally anhydrous minerals in a silica-rich system at the top lower mantle. *Earth and Planetary Science Letters*, *660*, 119360. https://doi.org/10.1016/j.epsl.2025.119360

Criniti, G., Ishii, T., Kurnosov, A., Glazyrin, K., & Boffa Ballaran, T. (2023). High-pressure phase transition and equation of state of hydrous Al-bearing silica. *American Mineralogist*, *108*(8), 1558–1568. https://doi.org/10.2138/am-2022-8546

Datchi, F., Dewaele, A., Loubeyre, P., Letoullec, R., Le Godec, Y., & Canny, B. (2007). Optical pressure sensors for high-pressure–high-temperature studies in a diamond anvil cell. *High Pressure Research*, *27*(4), 447–463. https://doi.org/10.1080/08957950701659593

Fei, Y., Ricolleau, A., Frank, M., Mibe, K., Shen, G., & Prakapenka, V. (2007). Toward an internally consistent pressure scale. *Proceedings of the National Academy of Sciences*, *104*(22), 9182–9186. https://doi.org/10.1073/pnas.0609013104

Fischer, R. A., Campbell, A. J., Chidester, B. A., Reaman, D. M., Thompson, E. C., Pigott, J. S., et al. (2018). Equations of state and phase boundary for stishovite and $CaCl_2$-type SiO_2. *American Mineralogist*, *103*(5), 792–802. https://doi.org/10.2138/am-2018-6267

Fukao, Y., & Obayashi, M. (2013). Subducted slabs stagnant above, penetrating through, and trapped below the 660 km discontinuity. *Journal of Geophysical Research: Solid Earth*, *118*(11), 5920–5938. https://doi.org/10.1002/2013jb010466

Ganguly, J., Freed, A. M., & Saxena, S. K. (2009). Density profiles of oceanic slabs and surrounding mantle: Integrated thermodynamic and thermal modeling, and implications for the fate of slabs at the 660 km discontinuity. *Physics of the Earth and Planetary Interiors*, *172*(3–4), 257–267. https://doi.org/10.1016/j.pepi.2008.10.005

Goes, S., Agrusta, R., van Hunen, J., & Garel, F. (2017). Subduction-transition zone interaction: A review. *Geosphere*, *13*(3), 644–664. https://doi.org/10.1130/ges01476.1

Haugland, S. M., Ritsema, J., Kaneshima, S., & Thorne, M. S. (2017). Estimate of the rigidity of eclogite in the lower mantle from waveform modeling of broadband S-to-P wave conversions. *Geophysical Research Letters*, *44*(23), 11778–11784. https://doi.org/10.1002/2017gl075463

He, X., & Zheng, Y. (2018). *S*-to-*P* conversions from mid-mantle slow scatterers in slab regions: Observations of deep/stagnated oceanic crust? *Pure and Applied Geophysics*, *175*(6), 2045–2055. https://doi.org/10.1007/s00024-017-1763-z

Hemley, R., Shu, J., Carpenter, M., Hu, J., Mao, H., & Kingma, K. (2000). Strain/order parameter coupling in the ferroelastic transition in dense SiO_2. *Solid State Communications*, *114*(10), 527–532. https://doi.org/10.1016/s0038-1098(00)00099-5

Hirose, K., Takafuji, N., Sata, N., & Ohishi, Y. (2005). Phase transition and density of subducted MORB crust in the lower mantle. *Earth and Planetary Science Letters*, *237*(1–2), 239–251. https://doi.org/10.1016/j.epsl.2005.06.035

Ishii, T., Criniti, G., Purevjav, N., Katsura, T., & Ohtani, E. (2024). Hydrogen partitioning between stishovite and hydrous phase δ: Implications for water cycle and distribution in the lower mantle. *Progress in Earth and Planetary Science*, *11*(1), 10. https://doi.org/10.1186/s40645-024-00615-0

Ishii, T., Miyajima, N., Criniti, G., Hu, Q., Glazyrin, K., & Katsura, T. (2022). High pressure-temperature phase relations of basaltic crust up to mid-mantle conditions. *Earth and Planetary Science Letters*, *584*, 117472. https://doi.org/10.1016/j.epsl.2022.117472

Ishii, T., Ohtani, E., & Shatskiy, A. (2022). Aluminum and hydrogen partitioning between bridgmanite and high-pressure hydrous phases: Implications for water storage in the lower mantle. *Earth and Planetary Science Letters*, *583*, 117441. https://doi.org/10.1016/j.epsl.2022.117441

Kaneshima, S. (2016). Seismic scatterers in the mid-lower mantle. *Physics of the Earth and Planetary Interiors*, *257*, 105–114. https://doi.org/10.1016/j.pepi.2016.05.004

Kaneshima, S. (2019). Seismic scatterers in the lower mantle near subduction zones. *Geophysical Journal International*, *219*(Supplement_1), S2–S20. https://doi.org/10.1093/gji/ggz241

Kaneshima, S. (2023). Mid-mantle seismic scatterers beneath the Samoan hotspot. *Physics of the Earth and Planetary Interiors*, *340*, 107034. https://doi.org/10.1016/j.pepi.2023.107034

Kaneshima, S., & Helffrich, G. (1999). Dipping low-velocity layer in the mid-lower mantle: Evidence for geochemical heterogeneity. *Science*, *283*(5409), 1888–1892. https://doi.org/10.1126/science.283.5409.1888

Kantor, I., Prakapenka, V., Kantor, A., Dera, P., Kurnosov, A., Sinogeikin, S., et al. (2012). BX90: A new diamond anvil cell design for X-ray diffraction and optical measurements. *Review of Scientific Instruments*, *83*(12). https://doi.org/10.1063/1.4768541

Katsura, T. (2022). A revised adiabatic temperature profile for the mantle. *Journal of Geophysical Research: Solid Earth*, *127*(2), e2021JB023562. https://doi.org/10.1029/2021jb023562

Kingma, K. J., Cohen, R. E., Hemley, R. J., & Mao, H.-K. (1995). Transformation of stishovite to a denser phase at lower-mantle pressures. *Nature*, *374*(6519), 243–245. https://doi.org/10.1038/374243a0

Krüger, F., Baumann, M., Scherbaum, F., & Weber, M. (2001). Mid mantle scatterers near the Mariana slab detected with a double array method. *Geophysical Research Letters*, *28*(4), 667–670. https://doi.org/10.1029/2000gl011570

Lakshtanov, D. L., Litasov, K. D., Sinogeikin, S. V., Hellwig, H., Li, J., Ohtani, E., & Bass, J. D. (2007). Effect of Al^{3+} and H^+ on the elastic properties of stishovite. *American Mineralogist*, *92*(7), 1026–1030. https://doi.org/10.2138/am.2007.2294

Lakshtanov, D. L., Sinogeikin, S. V., Litasov, K. D., Prakapenka, V. B., Hellwig, H., Wang, J., et al. (2007). The post-stishovite phase transition in hydrous alumina-bearing SiO_2 in the lower mantle of the earth. *Proceedings of the National Academy of Sciences*, *104*(34), 13588–13590. https://doi.org/10.1073/pnas.0706113104

Li, J., Chen, S., He, X., Wang, W., & Yang, F. (2022). Mid-lower mantle scatterers: Detection methods, research progress and prospect. *Reviews of Geophysics and Planetary Physics*, *53*, 1–16.

Li, J., & Yuen, D. A. (2014). Mid-mantle heterogeneities associated with Izanagi plate: Implications for regional mantle viscosity. *Earth and Planetary Science Letters*, *385*, 137–144. https://doi.org/10.1016/j.epsl.2013.10.042

Litasov, K. D., Kagi, H., Shatskiy, A., Ohtani, E., Lakshtanov, D. L., Bass, J. D., & Ito, E. (2007). High hydrogen solubility in Al-rich stishovite and water transport in the lower mantle. *Earth and Planetary Science Letters*, *262*(3–4), 620–634. https://doi.org/10.1016/j.epsl.2007.08.015

Liu, X. N., Matsukage, K., Nishihara, Y., Suzuki, T., & Takahashi, E. (2019). Stability of the hydrous phases of Al-rich phase D and Al-rich phase H in deep subducted oceanic crust. *American Mineralogist*, *104*(1), 64–72. https://doi.org/10.2138/am-2019-6559

Niu, F. (2014). Distinct compositional thin layers at mid-mantle depths beneath northeast China revealed by the USArray. *Earth and Planetary Science Letters*, *402*, 305–312. https://doi.org/10.1016/j.epsl.2013.02.015

Niu, F., Kawakatsu, H., & Fukao, Y. (2003). Seismic evidence for a chemical heterogeneity in the midmantle: A strong and slightly dipping seismic reflector beneath the Mariana subduction zone. *Journal of Geophysical Research*, *108*(B9). https://doi.org/10.1029/2002jb002384

Nomura, R., Hirose, K., Sata, N., & Ohishi, Y. (2010). Precise determination of post-stishovite phase transition boundary and implications for seismic heterogeneities in the mid-lower mantle. *Physics of the Earth and Planetary Interiors*, *183*(1–2), 104–109. https://doi.org/10.1016/j.pepi.2010.08.004

Ono, S., Hirose, K., Murakami, M., & Isshiki, M. (2002). Post-stishovite phase boundary in SiO_2 determined by in situ X-ray observations. *Earth and Planetary Science Letters*, *197*(3–4), 187–192. https://doi.org/10.1016/s0012-821x(02)00479-x

Ono, S., Ito, E., & Katsura, T. (2001). Mineralogy of subducted basaltic crust (MORB) from 25 to 37 GPa, and chemical heterogeneity of the lower mantle. *Earth and Planetary Science Letters*, *190*(1–2), 57–63. https://doi.org/10.1016/s0012-821x(01)00375-2

Paterson, M. (1982). The determination of hydroxyl by infrared absorption in quartz, silicate glasses and similar materials. *Bulletin de Mineralogie*, *105*(1), 20–29. https://doi.org/10.3406/bulmi.1982.7582

Pawley, A. R., McMillan, P. F., & Holloway, J. R. (1993). Hydrogen in stishovite, with implications for mantle water content. *Science*, *261*(5124), 1024–1026. https://doi.org/10.1126/science.261.5124.1024

Ricolleau, A., Perrillat, J. P., Fiquet, G., Daniel, I., Matas, J., Addad, A., et al. (2010). Phase relations and equation of state of a natural MORB: Implications for the density profile of subducted oceanic crust in the Earth's lower mantle. *Journal of Geophysical Research*, *115*(B8). https://doi.org/10.1029/2009jb006709

Rost, S., Garnero, E. J., & Williams, Q. (2008). Seismic array detection of subducted oceanic crust in the lower mantle. *Journal of Geophysical Research*, *113*(B6). https://doi.org/10.1029/2007jb005263

Shieh, S. R., Duffy, T. S., & Shen, G. (2005). X-ray diffraction study of phase stability in SiO_2 at deep mantle conditions. *Earth and Planetary Science Letters*, *235*(1–2), 273–282. https://doi.org/10.1016/j.epsl.2005.04.004

Sinogeikin, S., Bass, J., Prakapenka, V., Lakshtanov, D., Shen, G., Sanchez-Valle, C., & Rivers, M. (2006). Brillouin spectrometer interfaced with synchrotron radiation for simultaneous X-ray density and acoustic velocity measurements. *Review of Scientific Instruments*, *77*(10). https://doi.org/10.1063/1.2360884

Vanacore, E., Niu, F., & Kawakatsu, H. (2006). Observations of the mid-mantle discontinuity beneath Indonesia from *S* to *P* converted waveforms. *Geophysical Research Letters*, *33*(4). https://doi.org/10.1029/2005gl025106

Wang, W., Xu, Y., Sun, D., Ni, S., Wentzcovitch, R., & Wu, Z. (2020). Velocity and density characteristics of subducted oceanic crust and the origin of lower-mantle heterogeneities. *Nature Communications*, *11*(1), 64. https://doi.org/10.1038/s41467-019-13720-2

Yamazaki, D., Ito, E., Yoshino, T., Tsujino, N., Yoneda, A., Guo, X., et al. (2014). Over 1 Mbar generation in the Kawai-type multianvil apparatus and its application to compression of $(Mg_{0.92}Fe_{0.08})SiO_3$ perovskite and stishovite. *Physics of the Earth and Planetary Interiors*, *228*, 262–267. https://doi.org/10.1016/j.pepi.2014.01.013

Yang, Z., & He, X. (2015). Oceanic crust in the mid-mantle beneath west-central Pacific subduction zones: Evidence from *S* to *P* converted waveforms. *Geophysical Journal International*, *203*(1), 541–547. https://doi.org/10.1093/gji/ggv314

Yu, Y., Zhang, Y., Li, L., Zhang, X., Wang, D., Mao, Z., et al. (2025). Unraveling the complex features of the seismic scatterers in the mid-lower mantle through phase transition of (Al, H)-bearing stishovite [Dataset]. *Zenodo*. https://10.5281/zenodo.15590899

Yuan, Y., Sun, D., Leng, W., & Wu, Z. (2021). Southeastward dipping mid-mantle heterogeneities beneath the sea of Okhotsk. *Earth and Planetary Science Letters*, *573*, 117151. https://doi.org/10.1016/j.epsl.2021.117151

Zhang, L., Li, J., Wang, T., Yang, F., & Chen, Q. F. (2020). Body waves retrieved from noise cross-correlation reveal lower mantle scatterers beneath the Northwest Pacific subduction zone. *Geophysical Research Letters*, *47*(19), e2020GL088846. https://doi.org/10.1029/2020gl088846

Zhang, Y., Chariton, S., He, J., Fu, S., Xu, F., Prakapenka, V. B., & Lin, J.-F. (2023). Atomistic insight into the ferroelastic post-stishovite transition by high-pressure single-crystal X-ray diffraction. *American Mineralogist: Journal of Earth and Planetary Materials*, *108*(1), 110–119. https://doi.org/10.2138/am-2022-8458

Zhang, Y., Fu, S., Karato, S. i., Okuchi, T., Chariton, S., Prakapenka, V. B., & Lin, J. F. (2022). Elasticity of hydrated Al-bearing stishovite and post-stishovite: Implications for understanding regional seismic V_S anomalies along subducting slabs in the lower mantle. *Journal of Geophysical Research: Solid Earth*, *127*(4), e2021JB023170. https://doi.org/10.1029/2021jb023170

Zhang, Y., Fu, S., Wang, B., & Lin, J.-F. (2021). Elasticity of a pseudoproper ferroelastic transition from stishovite to post-stishovite at high pressure. *Physical Review Letters*, *126*(2), 025701. https://doi.org/10.1103/physrevlett.126.025701

References From the Supporting Information

Buchen, J., Marquardt, H., Schulze, K., Speziale, S., Boffa Ballaran, T., Nishiyama, N., & Hanfland, M. (2018). Equation of state of polycrystalline stishovite across the tetragonal-orthorhombic phase transition. *Journal of Geophysical Research: Solid Earth*, *123*(9), 7347–7360. https://doi.org/10.1029/2018jb015835

Ishii, T., Criniti, G., Ohtani, E., Purevjav, N., Fei, H., Katsura, T., & Mao, H.-K. (2022). Superhydrous aluminous silica phases as major water hosts in high-temperature lower mantle. *Proceedings of the National Academy of Sciences*, *119*(44), e2211243119. https://doi.org/10.1073/pnas.2211243119

Nisr, C., Leinenweber, K., Prakapenka, V., Prescher, C., Tkachev, S., & Shim, S. H. D. (2017). Phase transition and equation of state of dense hydrous silica up to 63 GPa. *Journal of Geophysical Research: Solid Earth*, *122*(9), 6972–6983. https://doi.org/10.1002/2017jb014055

Ono, S., Suto, T., Hirose, K., Kuwayama, Y., Komabayashi, T., & Kikegawa, T. (2002). Equation of state of Al-bearing stishovite to 40 GPa at 300 K. *American Mineralogist*, *87*(10), 1486–1489.